

# Remote magnon-phonon entanglement in the waveguide-magnomechanics

Shi-fan Qi<sup>1,\*</sup> and Fan Li<sup>1</sup>

<sup>1</sup>*College of Physics and Hebei Key Laboratory of Photophysics Research and Application, Hebei Normal University, Shijiazhuang 050024, China*

Generating long-distance quantum entanglement is crucial for advancing quantum information processing. In this work, we propose a protocol for generating remote magnon-phonon entanglement in a hybrid waveguide-magnomechanical system, where multiple spatially separated magnon modes couple to a common waveguide while interacting with their respective phonon modes. By applying tailored pulsed drives and engineering the magnomechanical interactions, our scheme enables the creation of diverse long-distance and dynamically stable entanglement. Beyond basic magnon-phonon two-mode entanglement, it supports genuine multimode entanglement between a single phonon and multiple magnons, bipartite entanglement between a single magnon and multiple phonons, as well as genuine four-mode entanglement involving two magnons and two phonons. Moreover, we show that dissipative magnon-magnon interactions mediated by traveling photons can generate substantially stronger remote entanglement than coherent couplings. Our work provides an experimentally feasible scheme for the remote generation of magnon-phonon entanglement.

## I. INTRODUCTION

Quantum entanglement between spatially separated systems is a vital resource for diverse quantum technologies [1], underpinning quantum networks [2, 3], quantum computing [4], and quantum communication [5]. Significant progress has been made in generating and distributing remote entanglement across various quantum platforms [6–11], yet its efficient realization remains a central and active topic of current research [12–17]. Extending beyond bipartite correlations, multipartite entanglement [18–20] serves as a key resource for diverse quantum-networking protocols, including quantum state sharing [21], quantum teleportation [22, 23], and quantum secret sharing [24]. Accordingly, it is of considerable importance to develop experimentally feasible schemes for preparing remote multipartite entanglement within specific physical platforms [25–29].

Hybrid quantum systems based on magnons in ferromagnetic crystals have attracted considerable interest owing to the long coherence times of spin ensembles [30, 31], providing a promising platform for entanglement generation and application. In particular, building on the cavity magnomechanical system [32–34], a yttrium iron garnet (YIG) sphere placed inside a microwave cavity enables the magnon mode to couple with photons via magnetic dipole interaction and with phonons via magnetostrictive forces, various schemes have been proposed for generating stable continuous-variable entanglement [35–38], including tripartite photon-magnon-phonon entanglement [39] and optical-magnon-microwave-phonon entanglement [40]. Furthermore, the hybrid cavity-magnon-qubit system [41, 42] provides an alternative route for realizing discrete-variable entanglement, such as photon-magnon-qubit GHZ state [43] and magnonic Bell [44] and NOON states [45]. However, these schemes are limited to local configurations and cannot generate remote entanglement. Recently, it has been shown that propagating microwave photons can mediate remote magnon-magnon cou-

pling [46], which can be exploited to generate remote bipartite magnon-magnon entanglement [47, 48].

The waveguide-magnon system [49–52] can induce long-distance magnon-magnon coupling, but it is generally ineffective for generating magnonic entanglement without external squeezing fields. To address this limitation and enable entanglement across different frequency modes, we combine the waveguide-magnon systems [52] with magnomechanical systems [32], forming a new hybrid waveguide-magnomechanical architecture. In this work, we analytically and numerically investigate the generation of entanglement between distant subsystems. By applying tailored driving fields and tuning the magnomechanical interactions, we realize several types of remote magnon-phonon entanglement, including two-mode magnon-phonon entanglement, genuine multimode entanglement between a single phonon and multiple magnon modes, multimode entanglement between a single magnon and multiple phonon modes, as well as genuine four-mode entanglement in a two-magnon-two-phonon system. Our results reveal that waveguide-mediated magnon-magnon interactions play a crucial role in generating the entanglement, with dissipative coupling outperforming coherent coupling for a fixed interaction strength.

The paper is organized as follows. In Sec. II, we introduce the waveguide-magnomechanical system and present the corresponding Hamiltonian. The system dynamics and the criteria to quantify entanglement are provided in Sec. III. Section IV presents the results on remote two-mode entanglement generation between magnon and phonon, multimode entanglement between a single magnon and multiple phonons, as well as between a single phonon and multiple magnons, and genuine four-mode entanglement in dual magnon-phonon systems. Finally, discussions and conclusions are provided in Sec. V.

## II. THE WAVEGUIDE-MAGNOMECHANICAL SYSTEM

As depicted in Fig. 1, the hybrid quantum system under consideration consists of  $N$  YIG spheres (which provide magnon modes) coupled to a microstrip waveguide at distinct

\* [qishifan@hebtu.edu.cn](mailto:qishifan@hebtu.edu.cn)

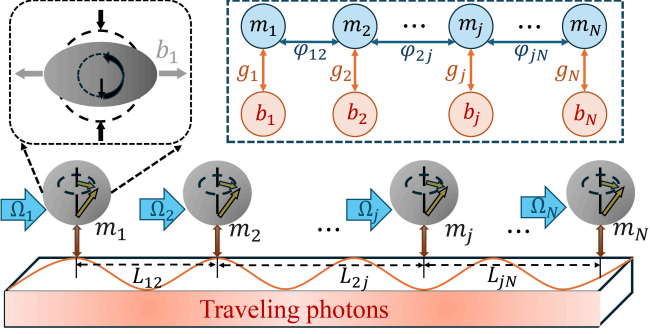


FIG. 1. Schematic diagram:  $N$  small YIG spheres (magnon modes) are coupled to a common waveguide, and the effective interactions between magnon modes  $m_j$  and  $m_l$  are mediated by traveling photons propagating in the waveguide. Moreover, the magnon mode  $m_j$  in each YIG sphere is driven by a strong control field with Rabi frequency  $\Omega_j$ . The upper left inset illustrates the magnetostrictive mechanism, where dynamic magnon magnetization (represented by vertical black arrows) induces mechanical deformation in the YIG sphere, thereby coupling to its phonon mode  $b_j$ . The right panel schematically depicts the mode couplings, where the magnon mode  $m_j$  couples to its phonon mode with strength  $g_j$ , while  $\varphi_{jk}$  denotes the quantum traveling phase between magnon modes  $m_j$  and  $m_k$ , which determines the form of the corresponding interaction.

locations [49]. The magnons interact with the photons in the waveguide via the Zeeman interaction and with their respective phonons (vibration modes of the YIG spheres) through the magnetostrictive interaction [32]. The system Hamiltonian can be written as

$$\begin{aligned}
 H_{\text{tot}} &= H_s + H_I + H_d, \\
 H_s &= \sum_{j=1}^N \omega_j m_j^\dagger m_j + \omega_b b_j^\dagger b_j + \tilde{g}_j m_j^\dagger m_j (b_j + b_j^\dagger), \\
 H_I &= -i \sum_{j=1}^{N-1} \sum_{l=j+1}^N \sqrt{\kappa_j \kappa_l} e^{i\varphi_{jl}} (m_j^\dagger m_l + m_j m_l^\dagger), \\
 H_d &= \sum_{j=1}^N \Omega_j (e^{-i\epsilon t} m_j^\dagger + e^{i\epsilon t} m_j),
 \end{aligned} \tag{1}$$

where  $H_s$  represents the  $N$  magnomechanical systems Hamiltonian,  $H_I$  denotes the interaction between magnon modes, and  $H_d$  describes the driving Hamiltonian.  $\omega_j$  is the transition frequency of magnon mode  $m_j$ , which is given by  $\omega_j = \tilde{\gamma} h_j$ , where  $\tilde{\gamma}$  is the gyromagnetic ratio and  $h_j$  is the external bias magnetic field, allowing for tuning via the external magnetic field.  $\omega_b$  denotes the transition frequency of the phonon modes (with the frequencies of various phonon modes assumed to be identical).  $\tilde{g}_j$  represents the single-excitation magnomechanical coupling strength, which can be tuned from 0 to 60 mHz by adjusting the direction of the bias field in recent experiments [32]. The coupling between magnon modes is mediated by traveling photons in the waveguide and consists of coherent and dissipative components, given by  $\sqrt{\kappa_j \kappa_l} \sin \varphi_{jl}$  and  $\sqrt{\kappa_j \kappa_l} \cos \varphi_{jl}$ , respectively. Here,  $\varphi_{jl}$  is the phase associated with the traveling

photons over the distance  $L_{jl}$ ,  $\kappa_j$  and  $\kappa_l$  are the radiative decay rates of magnons  $m_j$  and  $m_l$  induced by the waveguide photons (see Appendix A for details). The Rabi frequency,  $\Omega_j = \tilde{\gamma} \sqrt{5N} B_j / 4$ , characterizes the amplitude of the external driving field with frequency  $\epsilon$ , where  $B_j$  is the magnetic field strength of the driving field and  $\bar{N}$  represents the total number of spins in the YIG sphere [30].

Under strong-driving fields, the system's dynamics can be linearized by writing the operators  $o_j = \langle o_j \rangle + \delta o_j$ ,  $o = m, b$ , where  $\langle o_j \rangle$  is the steady amplitude of mode  $o_j$  and  $\delta o_j$  is the corresponding fluctuation operator. After the standard linearization approximation [26], the system Hamiltonian in Eq. (1) turns into

$$\begin{aligned}
 H &= \sum_{j=1}^N \Delta_j m_j^\dagger m_j + \omega_b b_j^\dagger b_j + g_j (m_j + m_j^\dagger) (b_j + b_j^\dagger) \\
 &\quad - i \sum_{j=1}^{N-1} \sum_{l=j+1}^N \sqrt{\kappa_j \kappa_l} e^{i\varphi_{jl}} (m_j^\dagger m_l + m_j m_l^\dagger),
 \end{aligned} \tag{2}$$

where  $\Delta_j = \omega_j - \epsilon$  is the detuning of magnon mode  $m_j$  and  $g_j = \tilde{g}_j \langle m_j \rangle$  is the driving-enhanced magnon-phonon coupling strength. Here, for simplicity, we apply the substitution  $\delta o_j \rightarrow o_j$ . Further details are provided in Appendix B.

### III. SYSTEM DYNAMICS AND ENTANGLEMENT CRITERION

In the framework of open quantum systems, under standard Markovian approximations and employing the quantum Langevin equation (QLE), the system dynamics governed by the Hamiltonian in Eq. (2) can be expressed in matrix form

$$\dot{u}(t) = A u(t) + \epsilon^{\text{in}}(t). \tag{3}$$

$u(t)$  is an operator vector, with components are given by  $u_{4j-3} = X_{m_j}$ ,  $u_{4j-2} = Y_{m_j}$ ,  $u_{4j-1} = X_{b_j}$ , and  $u_{4j} = Y_{b_j}$  for  $j = 1, 2, \dots, N$ , where  $u_j$  denotes the  $j$ -th component of  $u(t)$ .  $X_{o_j} = (o_j + o_j^\dagger)/\sqrt{2}$  and  $Y_{o_j} = (o_j - o_j^\dagger)/i\sqrt{2}$  are the quadrature operators of mode  $o_j$  with  $o = m, b$ . The drift matrix  $A$  is a square matrix of size  $4N \times 4N$ , whose elements can be expressed as

$$\begin{aligned}
 A_{4j-3,4j-2} &= -A_{4j-2,4j-3} = \Delta_j, \\
 A_{4j-1,4j} &= -A_{4j,4j-1} = \omega_b, \\
 A_{4j-3,4j-3} &= A_{4j-2,4j-2} = -\tilde{\kappa}_j, \\
 A_{4j-1,4j-1} &= A_{4j,4j} = -\kappa_b, \\
 A_{4j-2,4j-1} &= A_{4j,4j-3} = -2g_j, \\
 A_{4j-3,4l-3} &= A_{4j-2,4l-2} = -\sqrt{\kappa_j \kappa_l} \cos \varphi_{jl}, \quad j < l, \\
 A_{4j-3,4l-2} &= -A_{4j-2,4l-3} = \sqrt{\kappa_j \kappa_l} \sin \varphi_{jl}, \quad j < l,
 \end{aligned} \tag{4}$$

where  $A_{jl}$  denotes the matrix elements in the  $j$ -th row and  $l$ -th column.  $\tilde{\kappa}_j \equiv \kappa_j + \gamma_j$ , with  $\gamma_j$  is the intrinsic decay rate of magnon mode  $m_j$ .  $\epsilon^{\text{in}}(t)$  is the vector of Gaussian noise operators, its elements are defined as  $\epsilon_{4j-3}^{\text{in}} = \tilde{X}_j^{\text{in}}$ ,  $\epsilon_{4j-2}^{\text{in}} =$

$\tilde{Y}_j^{\text{in}}$ ,  $\epsilon_{4j-1}^{\text{in}} = X_{b_j}^{\text{in}}$ ,  $\epsilon_{4j}^{\text{in}} = Y_{b_j}^{\text{in}}$ , with  $\tilde{X}_j^{\text{in}} \equiv \sqrt{2\tilde{\kappa}_j}X_{m_j}^{\text{in}} + \sum_{l \neq j}^N \sqrt{2\Gamma_{jl}}X_{m_l}^{\text{in}}$  and  $\tilde{Y}_j^{\text{in}} \equiv \sqrt{2\tilde{\kappa}_j}Y_{m_j}^{\text{in}} + \sum_{l \neq j}^N \sqrt{2\Gamma_{jl}}Y_{m_l}^{\text{in}}$ , where  $\Gamma_{jl} \equiv \sqrt{\kappa_j\kappa_l} \cos \varphi_{jl}$ . The quadrature noise components are defined as  $X_{o_j}^{\text{in}} = (o_{j\text{in}} + o_{j\text{in}}^{\dagger})/\sqrt{2}$  and  $Y_{o_j}^{\text{in}} = (o_{j\text{in}} - o_{j\text{in}}^{\dagger})/i\sqrt{2}$ .  $m_{j\text{in}}$  and  $b_{j\text{in}}$  are the input noise operators for  $m_j$  and  $b_j$ , respectively, characterized by their corresponding covariance functions:  $\langle m_{j\text{in}}^{\dagger}(t)m_{j\text{in}}(t') \rangle = \bar{n}\delta(t - t')$  and  $\langle b_{j\text{in}}^{\dagger}(t)b_{j\text{in}}(t') \rangle = \bar{n}_b\delta(t - t')$ .  $\bar{n}$  and  $\bar{n}_b$  represent the mean populations at thermal equilibrium for the magnon and phonon modes, respectively. The derivations are provided in Appendix B and Eq. (3) is the matrix form of Eq. (B4).

Given the condition that all modes are initially occupied at their respective thermal states, the dynamics of the hybrid system can be fully described by the covariance matrix (CM)  $V(t)$  with dimension  $4N \times 4N$ . Via the QLE shown in Eq. (3), the CM  $V(t)$  satisfies

$$\dot{V}(t) = AV(t) + V(t)A^T + D, \quad (5)$$

where the elements of  $V$  are defined as  $V_{jl} = \langle u_j(t)u_l(t) + u_l(t)u_j(t) \rangle/2$ . The diffusion matrix  $D$  can be derived as

$$\begin{aligned} D_{4j-3,4j-3} &= D_{4j-2,4j-2} = \tilde{\kappa}_j(2\bar{n} + 1), \\ D_{4j-1,4j-1} &= D_{4j,4j} = \kappa_b(2\bar{n}_b + 1), \\ D_{4j-3,4l-3} &= D_{4j-2,4l-2} = \Gamma_{jl}(2\bar{n} + 1), \quad j < l, \end{aligned} \quad (6)$$

via its definitions  $D_{jl} = \langle \epsilon_j^{\text{in}}(t)\epsilon_l^{\text{in}}(t) + \epsilon_l^{\text{in}}(t)\epsilon_j^{\text{in}}(t) \rangle/2$ . With the initial condition,  $V_{4j-3,4j-3}(0) = V_{4j-2,4j-2}(0) = \bar{n} + 1/2$  and  $V_{4j-1,4j-1}(0) = V_{4j,4j}(0) = \bar{n}_b + 1/2$ , the CM  $V(t)$  can be obtained numerically by Eq. (5).

The logarithmic negativity (LN) are used to quantify the bipartite quantum entanglement between modes  $o$  and  $p$  in this hybrid system, which is defined as [53–55]

$$E_{o|p} \equiv \max[0, -\ln(2\tilde{e}_{o|p})], \quad (7)$$

where  $\tilde{e}_{o|p} = \min\{\text{eig}|i\sigma_2\tilde{V}_4|\}$  (with the symplectic matrix  $\sigma_2 = \bigoplus_{j=1}^2 i\sigma_y$  and  $\sigma_y$  is the  $y$ -Pauli matrix) is the minimum symplectic eigenvalue of the CM  $\tilde{V}_4 = P_{o|p}V_4P_{o|p}$ . Here,  $\tilde{V}_4$  is the  $4 \times 4$  CM of two-mode subsystems, obtained by removing the rows and columns corresponding to the uninteresting modes of  $V$ , and  $P_{o|p} = \text{Diag}[1, -1, 1, 1]$  is the matrix that realizes partial transposition at  $V_4$ . To calculate the one-mode-versus-multi-mode LN,  $E_{o|p_1p_2\dots p_n}$ , one simply follows the definition in Eq. (7), replacing  $\sigma_2 = \bigoplus_{j=1}^2 i\sigma_y$  with  $\sigma_n = \bigoplus_{j=1}^n i\sigma_y$ , and replacing  $\tilde{V}_4 = P_{o|p}V_4P_{o|p}$  with  $\tilde{V} = P_{o|p_1p_2\dots p_n}V P_{o|p_1p_2\dots p_n}$ , where  $P_{o|p_1p_2\dots p_n} = \text{Diag}[1, -1, 1, 1 \dots 1, 1]$  is the partial transposition matrix with dimension  $2n + 2$ . Similarly, for the two-mode-vs-two-mode LN  $E_{o_1o_2|p_1p_2}$ , the partial transposition matrix becomes  $P_{o_1o_2|p_1p_2} = \text{Diag}[1, -1, 1, -1, 1, 1, 1, 1]$  and the LN is given by  $E_{o_1o_2|p_1p_2} = \sum_j \max[0, -\ln(2\tilde{e}_j)]$ , where  $\tilde{e}_j = \text{eig}|i\sigma_4\tilde{V}_8|$  is the symplectic eigenvalue of the CM  $\tilde{V}_8 = P_{o_1o_2|p_1p_2}V P_{o_1o_2|p_1p_2}$ . Consequently, one can obtain the time-dependent LNs for all the above bipartitions once the system CM is numerically calculated using Eq. (5).

#### IV. NUMERICAL RESULTS ABOUT REMOTE MAGNON-PHONON ENTANGLEMENT

The preceding analysis provides a theoretical framework for investigating entanglement generation in this hybrid system. We now apply it to concrete models to realize remote magnon-phonon two-mode entanglement, multimode entanglement, and genuine four-mode entanglement.

##### A. Two-mode entanglement

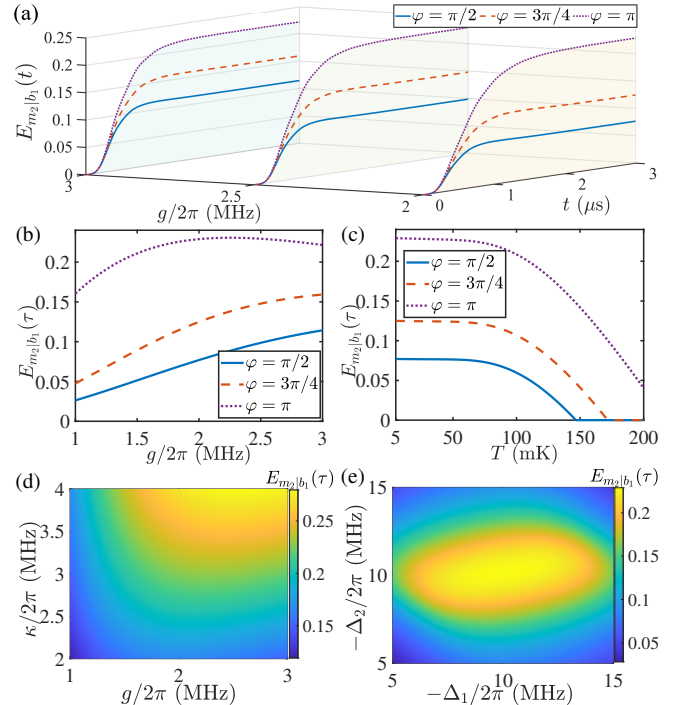


FIG. 2. (a) Time evolution of the LN quantifying bipartite entanglement between modes  $m_2$  and  $b_1$ , denoted as  $E_{m_2|b_1}(t)$ , under varying driving-enhanced magnomechanical coupling strength  $g$  and quantum phase  $\varphi$ . (b) LN  $E_{m_2|b_1}$  at a fixed time  $\tau$  as a function of  $g$  under different values of  $\varphi$ . (c)  $E_{m_2|b_1}(\tau)$  as a function of temperature  $T$  for different  $\varphi$ . (d)  $E_{m_2|b_1}(\tau)$  in the coupling strength  $g$  and decay rate  $\kappa$  parameter space. (e)  $E_{m_2|b_1}(\tau)$  in the parameter space spanned by magnon detunings  $\Delta_1$  and  $\Delta_2$ . For (b)–(e), the evolution time is set to  $\tau = 3 \mu\text{s}$ . The temperature is  $T = 10 \text{ mK}$ , except for (c).  $\kappa/2\pi = 3 \text{ MHz}$  except for (d).  $\varphi = \pi$  for (d) and (e).  $\Delta_1/2\pi = \Delta_2/2\pi = -10 \text{ MHz}$  for (a)–(d). Other parameters are set as  $\omega_b/2\pi = 10 \text{ MHz}$ ,  $\epsilon/2\pi = 10 \text{ GHz}$ ,  $\kappa_b/2\pi = 100 \text{ Hz}$ ,  $\gamma/2\pi = 1 \text{ MHz}$ , and  $g_2 = 0$ .

We first consider the process of remotely preparing entanglement between a single magnon and a single phonon, corresponding to a system with  $N = 2$  YIG spheres. The parameters are chosen as  $\Delta_1 = \Delta_2 = -\omega_b$ ,  $\varphi_{12} = \varphi$ ,  $\kappa_1 = \kappa_2 = \kappa$ ,  $g_1 = g$ , and  $g_2 = 0$ . Under these conditions, in the rotating-frame defined by the free Hamiltonian, applying the rotating-wave approximation to Eq. (2) yields the effective Hamiltonian

nian

$$H_{\text{eff}} = g(m_1^\dagger b_1^\dagger + mb) - i\kappa e^{i\varphi} (m_1^\dagger m_2 + m_1 m_2^\dagger). \quad (8)$$

The parametric down-conversion process, corresponding to the term  $m_1^\dagger b_1^\dagger + \text{h.c.}$ , generates quantum entanglement between  $m_1$  and  $b_1$ . Meanwhile, the beam-split interaction, i.e.,  $m_1^\dagger m_2 + \text{h.c.}$ , enables the transfer of this entanglement from the subsystem  $m_1 - b_1$  to the remote bipartite subsystem  $m_2 - b_1$ . In addition, throughout the discussion we neglect integer multiples of  $2\pi$  in the traveling phase, identifying  $2k\pi + \varphi \equiv \varphi$ .

In Fig. 2(a), the dynamical generation of remote bipartite magnon-phonon entanglement, denoted by  $E_{m_2|b_1}(t)$ , is illustrated for various values of the magnomechanical coupling strength  $g$  and traveling phase  $\varphi$ . It is observed that, irrespective of the values of  $g$  and  $\varphi$ , the LN  $E_{m_2|b_1}$  gradually converges to a steady value over time, signifying the establishment of stable entanglement within the two modes  $m_2$  and  $b_1$ . To examine the impact of parameters on entanglement generation, the LN  $E_{m_2|b_1}(\tau)$  at  $\tau = 2 \mu\text{s}$  is shown in Figs. 2(b)-(e). As seen in Fig. 2(b), for a fixed  $g$ ,  $E_{m_2|b_1}(\tau)$  is maximized at  $\varphi = \pi$ , corresponding to purely dissipative coupling. This exceeds the values at  $\varphi = 3\pi/4$  (mixed dissipative and coherent coupling) and  $\varphi = \pi/2$  (purely coherent coupling). Additionally, for  $\varphi = \pi/2$ ,  $E_{m_2|b_1}(\tau)$  increases with coupling strength  $g$ , whereas for  $\varphi = \pi$ , an optimal coupling range of  $1.9 \text{ MHz} \leq g/2\pi \leq 2.3 \text{ MHz}$  produces a higher LN. Fig. 2(c) presents similar behavior, at a fixed temperature, the LN reaches its maximum for  $\varphi = \pi$ , an intermediate value for  $\varphi = 3\pi/4$ , and its minimum for  $\varphi = \pi/2$ . Notably, the system at  $\varphi = \pi$  exhibits more resilience to thermal noise, with  $E_{m_2|b_1}(\tau) \approx 0.04$  even at  $T = 200 \text{ mK}$ , while the LNs for  $\varphi = \pi/2$  and  $\varphi = 3\pi/4$  vanishes at lower temperatures.

Figure 2(d) shows the LN  $E_{m_2|b_1}(\tau)$  versus the coupling strength  $g$  and magnon decay rate  $\kappa$ . The entanglement increases with both parameters and exceeds 0.25 for  $g/2\pi \geq 2 \text{ MHz}$  and  $\kappa/2\pi \geq 3.5 \text{ MHz}$ . To assess the robustness of the proposed scheme against detuning imperfections, we further analyze the entanglement behavior under finite magnon detunings, as shown in Fig. 2(e). Specifically, Fig. 2(e) displays  $E_{m_2|b_1}(\tau)$  in the parameter space spanned by  $\Delta_1$  and  $\Delta_2$ , revealing an optimal region for  $-1.2\omega_b \leq \Delta_{1,2} \leq -0.8\omega_b$ , with a slightly broader tolerance for  $\Delta_1$  than for  $\Delta_2$ .

## B. Multimode entanglement

In the preceding section, we demonstrated the generation of remote entanglement between a single magnon mode and a single phonon mode. We now turn our attention to the feasibility of generating remote multipartite entangled states involving magnons and phonons. For simplicity and without loss of generality, all magnon modes are assumed to have identical detunings and identical decay rates, i.e.,  $\Delta_1 = \Delta_2 = \dots = \Delta_N = \Delta$  and  $\kappa_1 = \kappa_2 = \dots = \kappa_N \equiv \kappa$ .

Specifically, we first consider the entanglement between a single phonon mode and  $N$  magnon modes. As shown in

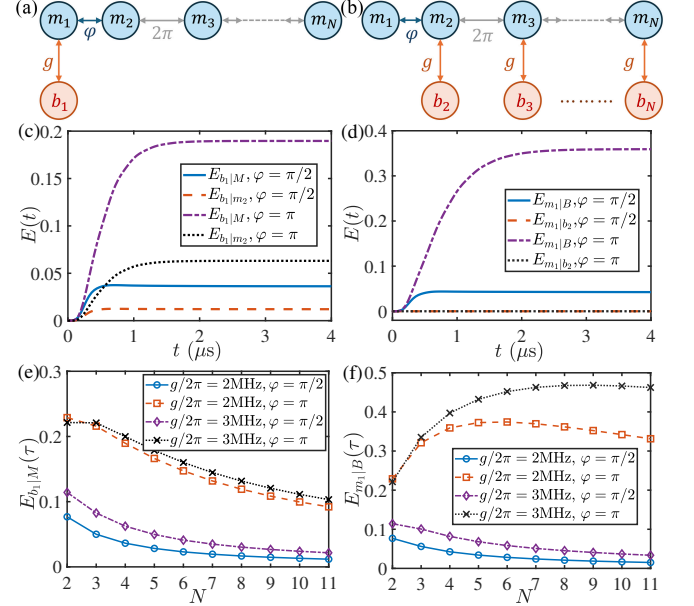


FIG. 3. [(a), (b)] Schematic diagrams illustrating the entanglement between a single phonon mode and  $N$  magnon modes, and between a single magnon mode and  $N$  phonon modes, respectively. [(c), (d)] Time evolution of the LNs  $E(t)$  under different phases for the models shown in (a) and (b), respectively. [(e), (f)] Dependence of the steady-state LNs  $E_{b_1|M}(\tau)$  and  $E_{m_1|B}(\tau)$  on the number of modes  $N$ , corresponding to the models in (a) and (b), respectively. Here,  $g/2\pi = 2 \text{ MHz}$  and  $N = 4$  for (c) and (d), while  $\tau = 4 \mu\text{s}$  for (e) and (f). Moreover,  $\Delta = -\omega_b$ , and all remaining parameters are identical to those used in Fig. 2(a).

Fig. 3(a), the parameters in Fig. 1 are chosen as  $g_1 = g$ ,  $g_2 = g_3 = \dots = g_N = 0$ ,  $\varphi_{12} = \varphi$ , and  $\varphi_{23} = \varphi_{34} = \dots = \varphi_{(N-1)N} = 2\pi$ . The corresponding system Hamiltonian and drift matrix are provided in Eqs. (C1) and (C2) of Appendix C, respectively. Numerical results are shown in Figs. 3(c) and (e). In Fig. 3(c), we present the dynamical evolution of the LNs for different phases  $\varphi$  at a fixed  $N = 4$ . Here,  $E_{b_1|M} \equiv E_{b_1|m_2 \dots m_N}$  quantifies the bipartite entanglement between the phonon mode  $b_1$  and all magnon modes except  $m_1$ . As the system evolves, all LNs approach their respective steady-state values asymptotically. Remarkably, when the interaction between  $m_1$  and  $m_2$  is purely dissipative ( $\varphi = \pi$ ), both  $E_{b_1|M}$  and  $E_{b_1|m_2}$  attain values exceeding those obtained under purely coherent coupling ( $\varphi = \pi/2$ ). This finding substantiates our earlier conclusion that dissipative interactions can enhance entanglement generation. Figure 3(e) illustrates the dependence of  $E_{b_1|M}$  at time  $\tau$  on the number of magnon modes  $N$ . For a fixed  $N$ , the LN  $E_{b_1|M}$  increases with the magnomechanical coupling strength  $g$ , irrespective of whether the interaction between  $m_1$  and  $m_2$  is coherent or dissipative. In addition,  $E_{b_1|M}$  decreases monotonically with increasing  $N$ . In the coherent-coupling regime ( $\varphi = \pi/2$ ), the rate of decrease gradually diminishes and eventually saturates, whereas in the dissipative-coupling regime ( $\varphi = \pi$ ), the decline remains nearly linear with an approximately constant slope. Moreover, due to the prescribed phase relations,

one can demonstrate that  $E_{b_1|m_2} = E_{b_1|m_3} = \dots = E_{b_1|m_N}$  and  $E_{b_1|M} = (N-1)E_{b_1|m_2}$ , which numerical results can be found in Fig. 5 of Appendix C. Moreover, since  $E_{b_1|m_j} > 0$  for any  $j = 2, \dots, N$ , it follows that no bipartition of the hybrid system is separable, indicating the presence of genuine remote multimode entanglement.

Furthermore, we investigate the entanglement between a single magnon mode and  $N$  phonon modes. As illustrated in Fig. 3(b), the parameters in Fig. 1 are chosen as  $g_1 = 0$ ,  $g_2 = g_3 = \dots = g_N = g$ ,  $\varphi_{12} = \varphi$ , and  $\varphi_{23} = \varphi_{34} = \dots = \varphi_{(N-1)N} = 2\pi$ . The corresponding system Hamiltonian and drift matrix are given in Eqs. (C3) and (C4) of Appendix C. Numerical results are presented in Figs. 3(d) and (f). The time evolutions of the LNs  $E_{m_1|B}$  and  $E_{m_1|b_2}$  at  $N = 4$  are shown in Fig. 3(d), where  $E_{m_1|B} \equiv E_{m_1|b_2 \dots b_N}$  denotes the LN between the magnon mode  $m_1$  and all phonon modes. Similar to the behavior in Fig. 3(c),  $E_{m_1|B}$  approaches a steady value in the long time limit, with its magnitude at  $\varphi = \pi$  exceeding that at  $\varphi = \pi/2$ . In contrast, the LN  $E_{m_1|b_2}$  remains zero throughout the entire evolution. The value of  $E_{m_1|B}$  at  $\tau = 4 \mu\text{s}$  is plotted in Fig. 3(f). In the coherent-coupling regime ( $\varphi = \pi/2$ ),  $E_{m_1|B}$  decreases monotonically with increasing  $N$ , with the decay rate gradually slowing and eventually saturating. In the dissipative-coupling regime ( $\varphi = \pi$ ),  $E_{m_1|B}$  initially increases and then decreases as  $N$  grows. For  $g/2\pi = 2 \text{ MHz}$ , the optimal range of magnon numbers is  $4 \leq N \leq 7$ , while for  $g/2\pi = 3 \text{ MHz}$ , it shifts to  $7 \leq N \leq 10$ . Thus, a stronger coupling  $g$  enables a larger ensemble of magnons to contribute to enhanced entanglement. Additional numerical results for other bipartitions are provided in Appendix C.

### C. Genuine four-mode entanglement

In this section, we consider a hybrid model consisting of four magnon modes and two phonon modes, where the parameters shown in Fig. 1 are fixed as  $N = 4$ ,  $g_1 = g_4 = g$ ,  $g_2 = g_3 = 0$ , and  $\varphi_{12} = \varphi_{34} = \varphi_{23} = 2\pi$ . The system Hamiltonian in Eq. (2) under this case can be simplified as

$$H = \sum_{j=1}^4 \Delta m_j^\dagger m_j + \sum_{j=1,4} \omega_b b_j^\dagger b_j + g(m_j + m_j^\dagger)(b_j + b_j^\dagger) - i\kappa \sum_{j=1}^3 \sum_{l=j+1}^4 (m_j^\dagger m_l + m_j m_l^\dagger). \quad (9)$$

Here, we assume  $\Delta_1 = \Delta_2 = \Delta_3 = \Delta_4 = \Delta$  and  $\kappa_1 = \kappa_2 = \kappa_3 = \kappa_4 = \kappa$ . The corresponding drift matrix  $A$  can be obtained from Eq. (4), after which the CM  $V(t)$  is calculated according to Eq. (5). Based on  $V(t)$ , the LNs characterizing the hybrid system are obtained, and the corresponding numerical results are shown in Fig. 4.

In Fig. 4(a), we plot the time evolution of the LNs  $E_{b_1|m_2m_3b_4}$  (blue solid line),  $E_{m_2|b_1m_3b_4}$  (red dashed line),  $E_{b_1m_2|m_3b_4}$  (purple dotted line), and  $E_{b_1b_4|m_2m_3}$  (black dash-dotted line) for the entire four-mode system. It is evident that all LNs converge to nonzero constants after suffi-

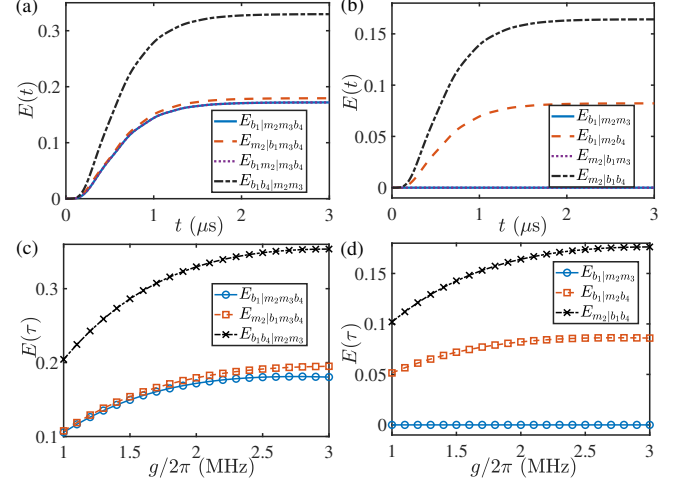


FIG. 4. [(a), (b)] The time evolution of the LNs  $E(t)$  associated with the genuine four-mode entanglement is shown, with  $g/2\pi = 2 \text{ MHz}$ . [(c), (d)] Dependence of the various LNs  $E(\tau)$  at fixed time  $\tau = 3 \mu\text{s}$  on the coupling strength  $g$ . Here,  $\Delta = -\omega_b$ , and the remaining parameters are identical to those in Fig. 2(a).

ciently long evolution. According to the symmetry relations given in Eq. (9), one obtains  $E_{b_4|b_1m_2m_3} = E_{b_1|m_2m_3b_4}$ ,  $E_{m_3|b_1m_2b_4} = E_{m_2|b_1m_3b_4}$ , and  $E_{b_1m_2|m_3b_4} = E_{b_1m_3|m_2b_4}$ . These results confirm that every possible bipartition of the four-mode system is entangled, evidencing the existence of genuine four-mode entanglement. The corresponding values of the LNs at  $\tau = 3 \mu\text{s}$  are plotted in Fig. 4(c). The LN  $E_{b_1m_2|m_3b_4}$  is not shown, as it is always equal to  $E_{b_1|m_2m_3b_4}$  for all parameter settings. The results indicate that the LNs approximately gradually increase as the coupling strength  $g$  is enhanced, although the rate of increase progressively slows for larger  $g$ . Notably, for  $g/2\pi > 2.8 \text{ MHz}$ ,  $E_{b_1|m_2m_3b_4}$  begins to decrease slightly, suggesting that further increases in  $g$  may not always enhance this LN and can instead reduce its value. Furthermore, the LNs satisfy the relation  $E_{b_1|m_2m_3b_4} = E_{b_1m_2|m_3b_4} < E_{m_2|b_1m_3b_4} < E_{b_1b_4|m_2m_3}$ , indicating that the bipartite entanglement between the two phonon modes and the two magnon modes is the strongest.

Moreover, we illustrate the bipartite entanglement present within a subsystem consisting of three modes in Fig. 4(b). As the system evolves, stable entanglement progressively develops between the phonon- $b_1$  and the magnon-phonon  $m_2b_4$ , as well as between magnon  $m_2$  and the biphonon  $b_1b_4$ . Specifically, it is observed that  $E_{b_1|m_2b_4} < E_{m_2|b_1b_4}$ . Conversely, no entanglement is generated between  $b_1$  and  $m_2m_3$ , nor between  $m_2$  and  $b_1m_3$  throughout the whole dynamics. More LNs can be similarly obtained by the symmetry relations, such as  $E_{b_1|m_2b_4} = E_{b_1|m_3b_4} = E_{b_4|m_2b_1} = E_{b_4|m_3b_1}$ . The corresponding values of  $E(\tau)$  are similarly shown in Fig. 4(d). One can observe that both  $E_{b_1|m_2b_4}$  and  $E_{m_2|b_1b_4}$  increase as the  $g$  is enhanced, and the increment diminishes progressively as  $g$  continues to increase. The values satisfy  $E_{b_1|m_2b_4} < E_{m_2|b_1b_4}$  and  $E_{b_1|m_2m_3} = 0$  for all coupling strengths. Furthermore, we also numerically demonstrate that  $E_{b_1|m_2} = E_{b_1|b_4} = E_{m_2|m_3} = 0$ , which indicates that an

arbitrary bipartition between one-mode and one-mode is separable. These results reveal that the phonon modes  $b_1$  and  $b_4$  behave as a collective subsystem capable of establishing entanglement with each magnon mode. The presence of the other phonon mode prevents the first phonon mode from entangling with the distinct magnon modes.

## V. DISCUSSION AND CONCLUSION

Our protocol is based on a hybrid waveguide-magnomechanical system that combines waveguide-magnon interactions [50–52] with magnomechanical coupling [32, 33]. All parameters used here are compatible with recent experiments. The magnon mode has a transition frequency of about 10 GHz, with an intrinsic decay rate of  $\gamma \sim 1$  MHz and a radiative decay rate of 2–4 MHz. The mechanical phonon mode operates near 10 MHz and has a much smaller decay rate of  $\kappa_b \sim 100$  Hz. The driving-enhanced magnomechanical coupling can reach  $g \sim 1 - 10$  MHz [34]. Recent studies further demonstrate that a single magnon mode can couple to a waveguide at two spatially separated points [49], enabling tunability of the radiative decay rate via the coupling distance. This provides additional control over entanglement and suggests promising directions for future studies. In addition to this system, our protocol is readily extendable to other quantum architectures, such as waveguide-optomechanical systems in which multiple optomechanical cavities are coupled to a common waveguide, enabling the generation of remote photon-phonon entanglement.

In summary, we have proposed a protocol for generating remote magnon-phonon entanglement in a waveguide-magnomechanical system, where magnons in spatially sep-

arated YIG spheres are coupled both to a common waveguide and to their local phonon modes. By appropriately engineering the driving-enhanced magnomechanical interactions, the scheme enables the generation of diverse forms of remote and dynamically stable entanglement. These include fundamental two-mode magnon-phonon entanglement, as well as more complex configurations such as genuine multimode entanglement between a single phonon and multiple magnons, bipartite entanglement between a single magnon and multiple phonons, and genuine four-mode entanglement involving two magnons and two phonons. Moreover, our analysis demonstrates that waveguide-photon-mediated dissipative magnon-magnon interactions yield substantially stronger entanglement than coherent coupling. Our work presents an interesting and experimentally feasible framework for generating remote entanglement in hybrid quantum systems.

## ACKNOWLEDGMENTS

We acknowledge financial support from the National Science Foundation of China (Grant No. 12404405), Hebei National Science Foundation (Grant No. A2025205030), and the Science Foundation of Hebei Normal University of China (Grant No. L2024B10).

## DATA AVAILABILITY

The data support the findings of this article are not publicly available. The data are available from the authors upon reasonable request.

## Appendix A: The magnon-magnon coupling mediated by waveguide photons

The waveguide-magnon system under consideration consists of  $N$  YIG spheres positioned at distinct positions along a one-dimensional microstrip waveguide [49–52]. The magnon modes provided by the YIG spheres couple with the traveling photons through magnetic dipole interaction. The total Hamiltonian of this system is given by

$$H = \sum_{j=1}^N \omega_j m_j^\dagger m_j + \int_{-\infty}^{+\infty} dk \tilde{\omega}_k a_k^\dagger a_k + \sum_{j=1}^N \int_{-\infty}^{+\infty} dk (G_j e^{-ikL_j} m_j a_k^\dagger + \text{h.c.}), \quad (\text{A1})$$

where  $a_k$  ( $a_k^\dagger$ ) is the annihilation (creation) operator of photons with transition frequency  $\omega_k$  and wave-vector  $k$ .  $G_j$  is the coupling strength between magnon-mode  $m_j$  and photon mode.  $L_j$  is the distance between the coupling points  $m_1$  and  $m_j$ , and  $L_1 = 0$ . With respect to the transformation  $U = \exp\{i \int_{-\infty}^{+\infty} dk \tilde{\omega}_k a_k^\dagger a_k\}$ , the original Hamiltonian in Eq. (A1) turns out to be

$$H_{\text{int}} = \sum_{j=1}^N \omega_j m_j^\dagger m_j + \sum_{j=1}^N \int_{-\infty}^{+\infty} dk (G_j e^{-ikL_j} e^{i\tilde{\omega}_k t} m_j a_k^\dagger + \text{h.c.}). \quad (\text{A2})$$

To study the coherent and dissipative dynamics of the multi-magnon subsystem, we eliminate the waveguide field using a standard procedure and derive the following master equation for the reduced density operator [56, 57], within the framework of

the Markovian approximation

$$\partial_t \rho(t) = - \int_0^\infty d\tau \text{Tr}_w [H_{\text{int}}(t), [H_{\text{int}}(t-\tau), \rho_w \otimes \rho(t)]], \quad (\text{A3})$$

where  $\text{Tr}_w$  represents a partial tracing over the waveguide degrees of freedom, and  $\rho_w = |0\rangle\langle 0|$  represents the initial vacuum state of the waveguide's photonic modes.  $\rho(t)$  is the density matrix of the multi-magnon modes. By substituting the interaction Hamiltonian  $H_{\text{int}}$  into Eq. (A3), we obtain

$$\begin{aligned} \partial_t \rho(t) = & -i \sum_{j=1}^N [\omega_j m_j^\dagger m_j, \rho(t)] - i \sum_{j=1}^{N-1} \sum_{l=j+1}^N \sqrt{\kappa_j \kappa_l} \sin \varphi_{jl} [m_j^\dagger m_l + m_l^\dagger m_j, \rho(t)] \\ & + \sum_{j=1}^N \kappa_j [2m_j \rho(t) m_j^\dagger - m_j^\dagger m_j \rho(t) - \rho(t) m_j^\dagger m_j] + \sum_{j=1}^{N-1} \sum_{l=j+1}^N \sqrt{\kappa_j \kappa_l} \cos \varphi_{jl} [2m_j \rho(t) m_l^\dagger - m_l^\dagger m_l \rho(t) - \rho(t) m_l^\dagger m_l], \end{aligned} \quad (\text{A4})$$

with

$$\kappa_j = G_j^2 \int_0^\infty d\tau \int_{-\infty}^{+\infty} dk e^{\pm i\omega_k \tau} = 2\pi G_j^2 / v_g, \quad (\text{A5})$$

by  $\int_{-\infty}^{+\infty} e^{\pm ikx} dx = 2\pi\delta(x)$ .  $\kappa_j$  represents the radiative decay rate associated with waveguide photons.  $\varphi_{jl} = \varphi_l - \varphi_j$ , with  $\varphi_j$  denotes the traveling phase,  $\varphi_1 = 0$  and the other phases satisfy  $\varphi_j = \omega_m L_j / v_g, j = 2, 3, \dots, N$ , and  $v_g$  represents the group speed of the microwave field.

From the master equation in Eq. (A4), it is evident that the coupling between magnon modes  $m_j$  and  $m_l$ , mediated by the waveguide photons, can be divided into two components, the dissipative coupling  $\sqrt{\kappa_j \kappa_l} \cos \varphi_{jl}$  and the coherent coupling  $\sqrt{\kappa_j \kappa_l} \sin \varphi_{jl}$ . The equation (A4) corresponds to a non-Hermitian Hamiltonian

$$H_m = \sum_{j=1}^N \omega_j m_j^\dagger m_j - i \sum_{j=1}^{N-1} \sum_{l=j+1}^N \sqrt{\kappa_j \kappa_l} e^{i\varphi_{jl}} (m_j^\dagger m_l + m_l^\dagger m_j). \quad (\text{A6})$$

## Appendix B: The derivation of the linearized Hamiltonian

Under the rotating frame with  $U = \exp[i\epsilon t \sum_{j=1}^N m_j^\dagger m_j]$ , the system Hamiltonian in Eq. (1) turns into

$$H'_{\text{tot}} = \sum_{j=1}^N \Delta_j m_j^\dagger m_j + \omega_b b_j^\dagger b_j + \tilde{g}_j m_j^\dagger m_j (b_j + b_j^\dagger) - i \sum_{j=1}^{N-1} \sum_{l=j+1}^N \sqrt{\kappa_j \kappa_l} e^{i\varphi_{jl}} (m_j^\dagger m_l + m_l^\dagger m_j) + \sum_{j=1}^N \Omega_j (m_j^\dagger + m_j), \quad (\text{B1})$$

where  $\Delta_j = \omega_j - \epsilon$  is the detuning of magnon  $m_j$ . Using the standard QLE and the master equation in Eq. (A4), the time evolution of the system operators under the Hamiltonian in Eq. (1) is given by

$$\begin{aligned} \dot{m}_j &= -(i\Delta_j + \tilde{\kappa}_j) m_j - i\tilde{g}_j m_j (b_j + b_j^\dagger) - \sum_{l \neq j}^N (\sqrt{\kappa_j \kappa_l} e^{i\varphi_{jl}} m_l - \sqrt{2\Gamma_{jl}} m_{l\text{in}}) + \sqrt{2\tilde{\kappa}_j} m_{j\text{in}} - i\Omega_j, \\ \dot{b}_j &= -(i\omega_b + \kappa_{b_j}) b_j - i\tilde{g}_j m_j^\dagger m_j + \sqrt{2\kappa_{b_j}} b_{j\text{in}}, \end{aligned} \quad (\text{B2})$$

where  $\tilde{\kappa}_j = \gamma_j + \kappa_j$  is the total decay rate of mode  $m_j$ , with  $\gamma_j$  denoting the intrinsic decay rate.  $\Gamma_{jl} \equiv \sqrt{\kappa_j \kappa_l} \cos \varphi_{jl}$  is the dissipative coupling strength between magnon modes  $m_j$  and  $m_l$ .  $m_{j\text{in}}$  and  $b_{j\text{in}}$  are the input noise operators for the magnon mode  $m_j$  and phonon mode  $b_j$ , respectively, which are characterized by their corresponding covariance functions:  $\langle o_{\text{in}}^\dagger(t) o_{\text{in}}(t') \rangle = \bar{n}_o \delta(t-t')$  and  $\langle o_{\text{in}}(t) o_{\text{in}}^\dagger(t') \rangle = [\bar{n}_o + 1] \delta(t-t')$ , under the Markovian approximation,  $\bar{n}_o = [\exp(\hbar\omega_o/k_B T) - 1]^{-1}$  is the mean population number at the thermal equilibrium state, with  $o = m_j, b_j$ . For simplicity and without loss of generality, in the following discussion and throughout the main manuscript, we assume  $\bar{n}_{m_j} = \bar{n}$ ,  $\kappa_{b_j} = \kappa_b$ , and  $\bar{n}_{b_j} = \bar{n}_b$ .

Under the condition of strong driving pulses  $\Omega_j$ , the magnon mode  $m_j$  has a large steady-state amplitude, i.e.,  $|\langle m_j \rangle| \gg 1$ . This allows us to linearize the system's dynamics around the constant values by expressing the operators as  $o = \langle o \rangle + \delta o$ , where  $o = m_j, b_j$  and  $\delta o$  represents the operator describing the quantum fluctuation. The constant values  $\langle o \rangle$  satisfy

$$\begin{aligned} (i\Delta_j + \tilde{\kappa}_j) \langle m_j \rangle + i\tilde{g}_j \langle m_j \rangle (\langle b_j \rangle + \langle b_j \rangle^*) + \sum_{l \neq j}^N i\sqrt{\kappa_j \kappa_l} e^{i\varphi_{jl}} \langle m_l \rangle + i\Omega_j &= 0, \\ (i\omega_b + \kappa_b) \langle b_j \rangle + i\tilde{g}_j |\langle m_j \rangle|^2 &= 0. \end{aligned} \quad (\text{B3})$$

When  $\Delta_j \gg \tilde{\kappa}_j, \tilde{g}_j$ , the expectation value  $\langle m_j \rangle$  is approximately given by  $\langle m_j \rangle \approx -\Omega_j/\Delta_j$ , which is purely real.

By substituting the constant values in Eq. (B3) into the equations in Eq. (B2) and ignoring all the higher-order terms of fluctuations, the QLEs describing the fluctuation operator  $\delta o$  can be described as

$$\begin{aligned}\dot{\delta m}_j &= -(i\Delta_j + \tilde{\kappa}_j)\delta m_j - i\tilde{g}_j\langle m_j \rangle(\delta b_j + \delta b_j^\dagger) - \sum_{l \neq j}^N (\sqrt{\kappa_j \kappa_l} e^{i\varphi_{jl}} \delta m_l - \sqrt{2\Gamma_{jl}} m_{l_{\text{in}}}) + \sqrt{2\tilde{\kappa}_j} m_{j_{\text{in}}}, \\ \dot{\delta b}_j &= -(i\omega_b + \kappa_b)\delta b_j - i\tilde{g}_j(\langle m_j \rangle^* \delta m_j + \langle m_j \rangle \delta m_j^\dagger) + \sqrt{2\kappa_b} b_{j_{\text{in}}}.\end{aligned}\quad (\text{B4})$$

The corresponding effective linearized Hamiltonian can be described as

$$H_{\text{lin}} = \sum_{j=1}^N \Delta_j \delta m_j^\dagger \delta m_j + \omega_b \delta b_j^\dagger \delta b_j + g_j (\delta m_j + \delta m_j^\dagger) (\delta b_j + \delta b_j^\dagger) - i \sum_{j=1}^{N-1} \sum_{l=j+1}^N \sqrt{\kappa_j \kappa_l} e^{i\varphi_{jl}} (\delta m_j^\dagger \delta m_l + \delta m_j \delta m_l^\dagger), \quad (\text{B5})$$

where  $g_j = \tilde{g}_j \langle m_j \rangle$ . It is the Hamiltonian in Eq. (2) in the main text. Here, the coupling strength  $g_j$  is assumed to be real-valued for simplicity and without loss of generality. Furthermore, for notational convenience, we adopt the convention  $\delta o \rightarrow o, o = m_j, b_j$  throughout the main text and subsequent analysis.

### Appendix C: Results for Remote Multimode Magnon-Phonon Entanglement

This appendix provides the system Hamiltonians and drift matrices for the models depicted in Figs. 3(a) and 3(b) of Sec. IV B. We first consider the hybrid model presented in Fig. 3(a), which is designed to generate remote entanglement between a single phonon and multiple magnons. The system parameters are chosen as  $g_1 = g, g_2 = g_3 = \dots = g_N = 0, \varphi_{12} = \varphi, \varphi_{23} = \varphi_{34} = \dots = \varphi_{(N-1)N} = 2\pi$ . The detunings and decay rates of all magnon modes are assumed to be identical, i.e.,  $\Delta_1 = \Delta_2 = \dots = \Delta_N = \Delta$  and  $\kappa_1 = \kappa_2 = \dots = \kappa_N \equiv \kappa$ . Under these conditions, the system Hamiltonian (2) turns into

$$H = \sum_{j=1}^N (\Delta m_j^\dagger m_j + \omega_b b_j^\dagger b_j) + g(m_1 + m_1^\dagger)(b_1 + b_1^\dagger) - i \sum_{j=2}^N \kappa e^{i\varphi} (m_1^\dagger m_j + m_1 m_j^\dagger) - i\kappa \sum_{j=2}^{N-1} \sum_{l=j+1}^N (m_j^\dagger m_l + m_j m_l^\dagger). \quad (\text{C1})$$

Under this condition, the operator vector  $u(t)$  in Eq. (3) can be simplified to  $u(t) = [X_{m_1}, Y_{m_1}, X_{b_1}, Y_{b_1}, X_{m_2}, Y_{m_2}, X_{m_3}, Y_{m_3}, \dots, X_{m_N}, Y_{m_N}]^T$ , and the corresponding drift matrix  $A$  in Eq. (3) turns into

$$A = \begin{bmatrix} -\tilde{\kappa} & \Delta & 0 & 0 & -\kappa \cos \varphi & \kappa \sin \varphi & -\kappa \cos \varphi & \kappa \sin \varphi & \dots & -\kappa \cos \varphi & \kappa \sin \varphi \\ -\Delta & -\tilde{\kappa} & -2g & 0 & -\kappa \sin \varphi & -\kappa \cos \varphi & -\kappa \sin \varphi & -\kappa \cos \varphi & \dots & -\kappa \sin \varphi & -\kappa \cos \varphi \\ 0 & 0 & -\kappa_b & \omega_b & 0 & 0 & 0 & 0 & \dots & 0 & 0 \\ -2g & 0 & -\omega_b & -\kappa_b & 0 & 0 & 0 & 0 & \dots & 0 & 0 \\ -\kappa \cos \varphi & \kappa \sin \varphi & 0 & 0 & -\tilde{\kappa} & \Delta & -\kappa & 0 & \dots & -\kappa & 0 \\ -\kappa \sin \varphi & -\kappa \cos \varphi & 0 & 0 & -\Delta & -\tilde{\kappa} & 0 & -\kappa & \dots & 0 & -\kappa \\ -\kappa \cos \varphi & \kappa \sin \varphi & 0 & 0 & -\kappa & 0 & -\tilde{\kappa} & \Delta & \dots & -\kappa & 0 \\ -\kappa \sin \varphi & -\kappa \cos \varphi & 0 & 0 & 0 & -\kappa & -\Delta & -\tilde{\kappa} & \dots & 0 & -\kappa \\ \vdots & \ddots & \vdots & \vdots \\ -\kappa \cos \varphi & \kappa \sin \varphi & 0 & 0 & -\kappa & 0 & -\kappa & 0 & \dots & -\tilde{\kappa} & \Delta \\ -\kappa \sin \varphi & -\kappa \cos \varphi & 0 & 0 & 0 & -\kappa & 0 & -\kappa & \dots & -\Delta & -\tilde{\kappa} \end{bmatrix} \quad (\text{C2})$$

with dimensions  $(2N + 2) \times (2N + 2)$ .  $\tilde{\kappa}$  is defined as the sum of the radiative decay rate  $\kappa$  and the intrinsic decay rate  $\gamma$  of magnon mode, i.e.,  $\tilde{\kappa} \equiv \kappa + \gamma$ . Subsequently, by utilizing the system dynamics described in Eq. (5), one can numerically calculate the CM  $V(t)$  for this hybrid system. Moreover, by applying the entanglement criterion in Eq. (7), the dynamical evolution of entanglement can be obtained, as depicted in Fig. 3(c) and (e) of the main manuscript.

In Fig. 5(a), we present the time evolution of the LNs  $E_{b_1|m_2m_3m_4}$ ,  $E_{b_1|m_2m_3}$ , and  $E_{b_1|m_2}$  for a system with  $N = 4$  YIGs. All quantities converge to steady-state values, satisfying the relations  $E_{b_1|m_2m_3} = 2E_{b_1|m_2}$  and  $E_{b_1|m_2m_3m_4} = 3E_{b_1|m_2}$ . Similarly, Fig. 5(b) shows the corresponding results for  $N = 5$ , where the steady-state values obey  $E_{b_1|m_2m_3m_4m_5} = 4E_{b_1|m_2}$  and  $E_{b_1|m_2m_3m_4} = 3E_{b_1|m_2}$ . Figure 5(c) shows the dependence of  $E_{b_1|M}$  and  $E_{b_1|m_2}$  at time  $\tau$  on the number of magnon modes  $N$ . Independent of the coupling strength  $g$ , the results clearly satisfy the relation  $E_{b_1|M} = (N-1)E_{b_1|m_2}$ , where  $E_{b_1|M} \equiv E_{b_1|m_2 \dots m_N}$ . Moreover, the imposed phase relations ensure that  $E_{b_1|m_2} = E_{b_1|m_3} = \dots = E_{b_1|m_N}$ . We thus conclude that the entanglement between a single phonon and multiple distant magnons equals the sum of the individual phonon-magnon entanglements. Furthermore, additional numerical analysis confirms that  $E_{m_j|m_l} = 0$  for all  $j, l = 2, \dots, N$  with  $j \neq l$ , indicating the absence of entanglement between magnon modes.

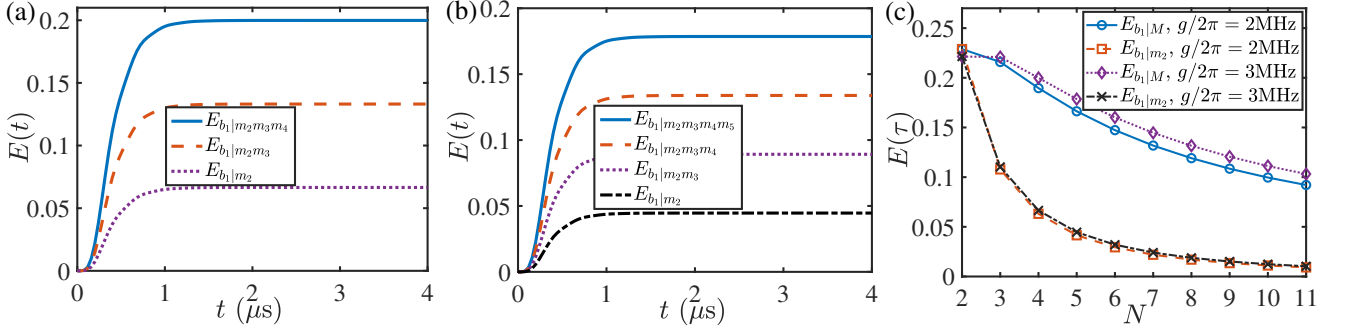


FIG. 5. [(a), (b)] Time evolution of the LNs  $E(t)$  for various bipartitions with  $N = 4$  and  $N = 5$ , respectively. The coupling strength is set to  $g/2\pi = 2$  MHz. (c) The LNs  $E_{b1|M} \equiv E_{b1|m_2 \dots m_N}$  and  $E_{b1|m_2}$  evaluated at time  $\tau = 4$   $\mu$ s as a function of the number of YIGs  $N$ . Here, the other parameters are set to  $\varphi = \pi$ ,  $\Delta = -\omega_b$ ,  $\omega_b/2\pi = 10$  MHz,  $\epsilon/2\pi = 10$  GHz,  $\kappa_b/2\pi = 100$  Hz,  $\kappa/2\pi = 3$  MHz,  $\gamma/2\pi = 1$  MHz, and  $T = 10$  mK.

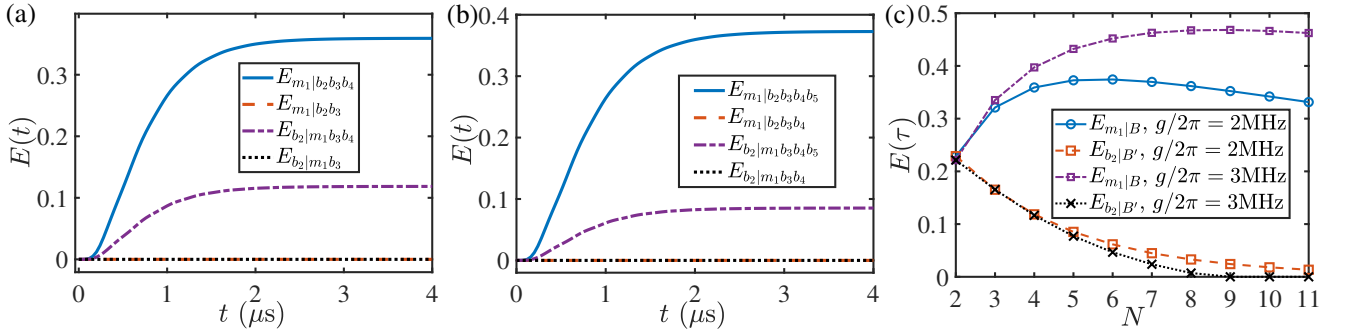


FIG. 6. [(a), (b)] Time evolution of the LNs  $E(t)$  for various bipartitions with  $N = 4$  and  $N = 5$ , respectively. The coupling strength is set to  $g/2\pi = 2$  MHz. (c) LNs  $E_{m1|B} \equiv E_{m1|b_2b_3 \dots b_N}$  and  $E_{b2|B'} \equiv E_{b2|m_1b_3 \dots b_N}$  evaluated at time  $\tau = 4$   $\mu$ s as a function of the number of YIGs  $N$ . Here, all other parameters are identical to those in Fig. 5.

Next, we consider the hybrid model presented in Fig. 3(b), which is designed to generate remote entanglement between a single magnon and multiple phonons. The system parameters are chosen as  $g_1 = 0$ ,  $g_2 = g_3 = \dots = g_N = g$ ,  $\varphi_{12} = \varphi$ ,  $\varphi_{23} = \varphi_{34} = \dots = \varphi_{(N-1)N} = 2\pi$ . Additionally, the detunings and decay rates of all magnon modes are assumed to be identical, namely,  $\Delta_1 = \Delta_2 = \dots = \Delta_N = \Delta$  and  $\kappa_1 = \kappa_2 = \dots = \kappa_N \equiv \kappa$ . Under these conditions, the system Hamiltonian in Eq. (2) simplifies into

$$H = \sum_{j=1}^N (\Delta m_j^\dagger m_j + \omega_b b_j^\dagger b_j) + \sum_{j=2}^N [g(m_j + m_j^\dagger)(b_j + b_j^\dagger) - i\kappa e^{i\varphi}(m_1^\dagger m_j + m_1 m_j^\dagger)] - i\kappa \sum_{j=2}^{N-1} \sum_{l=j+1}^N (m_j^\dagger m_l + m_j m_l^\dagger). \quad (C3)$$

Under this case, the operator vector  $u(t)$  in Eq. (3) reduces into  $u(t) = [X_{m_1}, Y_{m_1}, X_{m_2}, Y_{m_2}, X_{b_2}, Y_{b_2}, \dots, X_{m_N}, Y_{m_N}, X_{b_N}, Y_{b_N}]^T$ , and the corresponding drift matrix  $A$  in Eq. (3) takes the form

$$A = \begin{bmatrix} -\tilde{\kappa} & \Delta & -\kappa \cos \varphi & \kappa \sin \varphi & 0 & 0 & \dots & -\kappa \cos \varphi & \kappa \sin \varphi & 0 & 0 \\ -\Delta & -\tilde{\kappa} & -\kappa \sin \varphi & -\kappa \cos \varphi & 0 & 0 & \dots & -\kappa \sin \varphi & -\kappa \cos \varphi & 0 & 0 \\ -\kappa \cos \varphi & \kappa \sin \varphi & -\tilde{\kappa} & \Delta & 0 & 0 & \dots & -\kappa & 0 & 0 & 0 \\ -\kappa \sin \varphi & -\kappa \cos \varphi & -\Delta & -\tilde{\kappa} & -2g & 0 & \dots & 0 & -\kappa & 0 & 0 \\ 0 & 0 & 0 & 0 & -\kappa_b & \omega_b & \dots & 0 & 0 & 0 & 0 \\ 0 & 0 & -2g & 0 & -\omega_b & -\kappa_b & \dots & 0 & 0 & 0 & 0 \\ \vdots & \ddots & \vdots & \vdots \\ -\kappa \cos \varphi & \kappa \sin \varphi & -\kappa & 0 & 0 & 0 & \dots & -\tilde{\kappa} & \Delta & 0 & 0 \\ -\kappa \sin \varphi & -\kappa \cos \varphi & 0 & -\kappa & 0 & 0 & \dots & -\Delta & -\tilde{\kappa} & -2g & 0 \\ 0 & 0 & 0 & 0 & 0 & 0 & \dots & 0 & 0 & -\kappa_b & \omega_b \\ 0 & 0 & 0 & 0 & 0 & 0 & \dots & -2g & 0 & -\omega_b & -\kappa_b \end{bmatrix} \quad (C4)$$

with dimensions  $(4N-2) \times (4N-2)$ . Subsequently, by utilizing the system dynamics described in Eq. (5), one can numerically

calculate the CM  $V(t)$  for the hybrid system. Moreover, by applying the entanglement criterion in Eq. (7), the dynamical evolution of entanglement can be derived, as depicted in Fig. 3(d) and (f) of the main text.

Figure 6(a) and (b) present the time evolution of various LNs for systems comprising  $N = 4$  and  $N = 5$  YIGs, respectively. For a fixed  $N$ , the LN between any single mode and the remainder of the system converges to a steady value after sufficiently long evolution. The other LNs, not shown in the figure, can be readily inferred from the previously established phase relations. Notably, the entanglement between a single magnon and the collective phonon modes (blue solid line) is considerably stronger than that between a single phonon and all other modes combined (red dashed line). In contrast, when the multipartite partition excludes any of the remaining modes, the corresponding entanglement remains identically zero throughout the entire evolution (purple dash-dotted and black dotted lines). This feature closely resembles that of a GHZ state, in which tracing out any individual subsystem completely destroys all entanglement, emphasizing the delicate and global nature of the quantum correlations in the system. In Fig. 6(c), the LNs at time  $\tau$  are plotted as functions of the total number of YIG spheres  $N$ . Here,  $E_{m_1|B} \equiv E_{m_1|b_2b_3\dots b_N}$  and  $E_{b_2|B'} \equiv E_{b_2|m_2b_3\dots b_N}$ . It is observed that a stronger magnomechanical coupling  $g$  enhances  $E_{m_1|B}$  while reducing  $E_{b_2|B'}$  for a fixed  $N$ . Moreover,  $E_{b_2|B'}$  decreases monotonically with increasing  $N$ . In particular, for a larger coupling strength  $g/2\pi = 3\text{MHz}$ ,  $E_{b_2|B'}$  vanishes when  $N \geq 9$ , indicating the absence of genuine multimode entanglement.

---

[1] H. K. Beukers, M. Pasini, H. Choi, D. Englund, R. Hanson, and J. Borregaard, *Remote-entanglement protocols for stationary qubits with photonic interfaces*, *PRX Quantum* **5**, 010202 (2024).

[2] H. Kimble, *The quantum internet*, *Nature (London)* **453**, 1023 (2008).

[3] P. van Loock and S. L. Braunstein, *Multipartite entanglement for continuous variables: A quantum teleportation network*, *Phys. Rev. Lett.* **84**, 3482 (2000).

[4] T. D. Ladd, F. Jelezko, R. Laflamme, Y. Nakamura, C. Monroe, and J. L. O'Brien, *Quantum computers*, *Nature (London)* **464**, 45 (2010).

[5] A. Reiserer and G. Rempe, *Cavity-based quantum networks with single atoms and optical photons*, *Rev. Mod. Phys.* **87**, 1379 (2015).

[6] P. S. Shah, F. Yang, C. Joshi, and M. Mirhosseini, *Stabilizing remote entanglement via waveguide dissipation*, *PRX Quantum* **5**, 030346 (2024).

[7] B. Abdo, W. Shanks, O. Jinka, J. R. Rozen, and J. Orcutt, *Teleportation and entanglement swapping of continuous quantum variables of microwave radiation*, *Phys. Rev. X* **15**, 031075 (2025).

[8] Y.-T. Chen, L. Du, Y. Zhang, L. Guo, J.-H. Wu, M. Artoni, and G. C. La Rocca, *Giant-atom effects on population and entanglement dynamics of rydberg atoms in the optical regime*, *Phys. Rev. Res.* **5**, 043135 (2023).

[9] A. Lingenfelter, M. Yao, A. Pocklington, Y.-X. Wang, A. Irfan, W. Pfaff, and A. A. Clerk, *Exact results for a boundary-driven double spin chain and resource-efficient remote entanglement stabilization*, *Phys. Rev. X* **14**, 021028 (2024).

[10] J. V. Rakonjac, G. Corrielli, D. Lago-Rivera, A. Seri, M. Mazzera, S. Grandi, R. Osellame, and H. d. Riedmatten, *Storage and analysis of light-matter entanglement in a fiber-integrated system*, *Sci. Adv.* **8**, eabn3919 (2022).

[11] J. Qiu, Y. Liu, L. Hu, Y. Wu, J. Niu, L. Zhang, W. Huang, Y. Chen, J. Li, S. Liu, Y. Zhong, L. Duan, and D. Yu, *Deterministic quantum state and gate teleportation between distant superconducting chips*, *Sci. Bull.* **70**, 351 (2025).

[12] H.-T. Tan, W.-M. Zhang, and G.-x. Li, *Entangling two distant nanocavities via a waveguide*, *Phys. Rev. A* **83**, 062310 (2011).

[13] C. Gonzalez-Ballester, E. Moreno, and F. J. Garcia-Vidal, *Generation, manipulation, and detection of two-qubit entangle-ment in waveguide qed*, *Phys. Rev. A* **89**, 042328 (2014).

[14] A. C. Santos and R. Bachelard, *Generation of maximally entangled long-lived states with giant atoms in a waveguide*, *Phys. Rev. Lett.* **130**, 053601 (2023).

[15] X.-L. Yin, H.-w. J. Lee, and G. Zhang, *Giant-atom dephasing dynamics and entanglement generation in a squeezed vacuum reservoir*, *Phys. Rev. A* **111**, 033707 (2025).

[16] J. Liu, Z.-q. Liu, Y. Cai, K.-J. Ma, Y. Sang, and L. Tan, *Entanglement transfer between giant atoms in waveguide-qed systems*, *Adv. Quantum Technol.* **8**, e2500044 (2025).

[17] J. Ghosh, K. Debnath, and S. K. Varshney, *Secure quantum communication via einstein-podolsky-rosen steering between remotely coupled optomechanical systems*, *Phys. Rev. A* **113**, 013521 (2026).

[18] A. R. R. Carvalho, F. Mintert, and A. Buchleitner, *Decoherence and multipartite entanglement*, *Phys. Rev. Lett.* **93**, 230501 (2004).

[19] M. Navascués, E. Wolfe, D. Rosset, and A. Pozas-Kerstjens, *Genuine network multipartite entanglement*, *Phys. Rev. Lett.* **125**, 240505 (2020).

[20] G. C. Santra, S. S. Roy, D. J. Egger, and P. Hauke, *Genuine multipartite entanglement in quantum optimization*, *Phys. Rev. A* **111**, 022434 (2025).

[21] A. M. Lance, T. Symul, W. P. Bowen, B. C. Sanders, and P. K. Lam, *Tripartite quantum state sharing*, *Phys. Rev. Lett.* **92**, 177903 (2004).

[22] J. Lee, H. Min, and S. D. Oh, *Multipartite entanglement for entanglement teleportation*, *Phys. Rev. A* **66**, 052318 (2002).

[23] N. Yonezawa, T. Aoki, and A. Furusawa, *Demonstration of a quantum teleportation network for continuous variables*, *Nature (London)* **431**, 430 (2024).

[24] R. Cleve, D. Gottesman, and H.-K. Lo, *How to share a quantum secret*, *Phys. Rev. Lett.* **83**, 648 (1999).

[25] C. W. Sandbo Chang, M. Simoen, J. Aumentado, C. Sabín, P. Forn-Díaz, A. M. Vadiraj, F. Quijandría, G. Johansson, I. Fuentes, and C. M. Wilson, *Generating multimode entangled microwaves with a superconducting parametric cavity*, *Phys. Rev. Appl.* **10**, 044019 (2018).

[26] M. Aspelmeyer, T. J. Kippenberg, and F. Marquardt, *Cavity optomechanics*, *Rev. Mod. Phys.* **86**, 1391 (2014).

[27] A. Blais, A. L. Grimsmo, S. M. Girvin, and A. Wallraff, *Circuit quantum electrodynamics*, *Rev. Mod. Phys.* **93**, 025005 (2021).

[28] G. Andersson, S. W. Jolin, M. Scigliuzzo, R. Borgani, M. O. Tholén, J. Rivera Hernández, V. Shumeiko, D. B. Haviland, and P. Delsing, *Squeezing and multimode entanglement of surface acoustic wave phonons*, *PRX Quantum* **3**, 010312 (2022).

[29] V. Krutyanskiy, M. Canteri, M. Meraner, V. Krcmarsky, and B. Lanyon, *Multimode ion-photon entanglement over 101 kilometers*, *PRX Quantum* **5**, 020308 (2024).

[30] B. Z. Rameshti, S. V. Kusminskiy, J. A. Haigh, K. Usami, D. Lachance-Quirion, Y. Nakamura, C.-M. Hu, H. X. Tang, G. E. Bauer, and Y. M. Blanter, *Cavity magnonics*, *Phys. Rep.* **979**, 1 (2022).

[31] H. Yuan, Y. Cao, A. Kamra, R. A. Duine, and P. Yan, *Quantum magnonics: When magnon spintronics meets quantum information science*, *Phys. Rep.* **965**, 1 (2022).

[32] X. Zhang, C.-L. Zou, L. Jiang, and H. Tang, *Cavity magnon-mechanics*, *Sci. Adv.* **2**, e1501286 (2016).

[33] R.-C. Shen, J. Li, Z.-Y. Fan, Y.-P. Wang, and J. Q. You, *Mechanical bistability in kerr-modified cavity magnomechanics*, *Phys. Rev. Lett.* **129**, 123601 (2022).

[34] X. Zuo, Z.-Y. Fan, H. Qian, M.-S. Ding, H. Tan, H. Xiong, and J. Li, *Cavity magnomechanics: from classical to quantum*, *New J. Phys.* **26**, 031201 (2024).

[35] S. Chakraborty and C. Das, *Nonreciprocal magnon-photon-phonon entanglement in cavity magnomechanics*, *Phys. Rev. A* **108**, 063704 (2023).

[36] B. Hussain, S. Qamar, and M. Irfan, *Entanglement enhancement in cavity magnomechanics by an optical parametric amplifier*, *Phys. Rev. A* **105**, 063704 (2022).

[37] S.-f. Qi and J. Jing, *Kerr-magnon-assisted asymptotic stationary photon-phonon squeezing*, *Phys. Rev. A* **111**, 013708 (2025).

[38] A. Kumar Chauhan, A. Kani, and J. Twamley, *Enhancing macroscopic multimode entanglement through many-body interactions in cavity magnomechanics*, *Phys. Rev. A* **111**, 033505 (2025).

[39] J. Li, S.-Y. Zhu, and G. S. Agarwal, *Magnon-photon-phonon entanglement in cavity magnomechanics*, *Phys. Rev. Lett.* **121**, 203601 (2018).

[40] Z.-Y. Fan, L. Qiu, S. Gröblacher, and J. Li, *Microwave-optics entanglement via cavity optomagnomechanics*, *Laser Photonics Rev.* **17**, 2200866 (2023).

[41] Y. Tabuchi, S. Ishino, A. Noguchi, T. Ishikawa, R. Yamazaki, K. Usami, and Y. Nakamura, *Coherent coupling between a ferromagnetic magnon and a superconducting qubit*, *Science* **349**, 405 (2015).

[42] D. Xu, X.-K. Gu, H.-K. Li, Y.-C. Weng, Y.-P. Wang, J. Li, H. Wang, S.-Y. Zhu, and J. Q. You, *Quantum control of a single magnon in a macroscopic spin system*, *Phys. Rev. Lett.* **130**, 193603 (2023).

[43] S.-f. Qi and J. Jing, *Generation of bell and greenberger-horne-zeilinger states from a hybrid qubit-photon-magnon system*, *Phys. Rev. A* **105**, 022624 (2022).

[44] D. Xu, X.-K. Gu, Y.-C. Weng, H.-K. Li, Y.-P. Wang, S.-Y. Zhu, and J. Q. You, *Macroscopic bell state between a millimeter-sized spin system and a superconducting qubit*, *Quantum Sci. Technol.* **9**, 035002 (2024).

[45] S.-f. Qi and J. Jing, *Floquet generation of a magnonic noon state*, *Phys. Rev. A* **107**, 013702 (2023).

[46] Y. Li, V. G. Yefremenko, M. Lisovenko, C. Trevillian, T. Polakovic, T. W. Cecil, P. S. Barry, J. Pearson, R. Divan, V. Tyberkevych, C. L. Chang, U. Welp, W.-K. Kwok, and V. Novosad, *Coherent coupling of two remote magnonic resonators mediated by superconducting circuits*, *Phys. Rev. Lett.* **128**, 047701 (2022).

[47] W.-J. Wu, Y.-P. Wang, J.-Z. Wu, J. Li, and J. Q. You, *Remote magnon entanglement between two massive ferrimagnetic spheres via cavity optomagnonics*, *Phys. Rev. A* **104**, 023711 (2021).

[48] J. Xie, H. Yuan, S. Ma, S. Gao, F. Li, and R. A. Duine, *Stationary quantum entanglement and steering between two distant macromagnets*, *Quantum Sci. Technol.* **8**, 035022 (2023).

[49] Z.-Q. Wang, Y.-P. Wang, J. Yao, R. Shen, W.-J. Wu, J. Qian, J. Li, S.-Y. Zhu, and J. You, *Giant spin ensembles in waveguide magnonics*, *Nat. Commun.* **13**, 7580 (2022).

[50] Y. Yang, J. Yao, Y. Xiao, P.-T. Fong, H.-K. Lau, and C.-M. Hu, *Anomalous long-distance coherence in critically driven cavity magnonics*, *Phys. Rev. Lett.* **132**, 206902 (2024).

[51] Z.-Q. Wang, Z.-Y. Wang, Y.-P. Wang, and J. Q. You, *Single-mode magnon-polariton lasing and amplification controlled by dissipative coupling*, *Phys. Rev. Lett.* **135**, 186704 (2025).

[52] J. Qian, Q. Hong, Z.-Y. Wang, W.-X. Wu, Y. Yang, C.-M. Hu, J.-Q. You, and Y.-p. Wang, *Unidirectional perfect absorption induced by chiral coupling in spin-momentum locked waveguide magnonics*, *Nat. Commun.* **16**, 8100 (2025).

[53] G. Vidal and R. F. Werner, *Computable measure of entanglement*, *Phys. Rev. A* **65**, 032314 (2002).

[54] G. Adesso and F. Illuminati, *Entanglement in continuous-variable systems: recent advances and current perspectives*, *J. Phys. A* **40**, 7821 (2007).

[55] G. Adesso, A. Serafini, and F. Illuminati, *Quantification and scaling of multipartite entanglement in continuous variable systems*, *Phys. Rev. Lett.* **93**, 220504 (2004).

[56] H. Breuer and F. Petruccione, *The Theory of Open Quantum Systems* (Oxford University Press, Oxford, 2002).

[57] G. Calajó, F. Ciccarello, D. Chang, and P. Rabl, *Atom-field dressed states in slow-light waveguide qed*, *Phys. Rev. A* **93**, 033833 (2016).